Broadband sound generation by confined turbulent jets

Zhaoyan Zhang, Luc Mongeau, and Steven H. Frankel

Citation: The Journal of the Acoustical Society of America **112**, 677 (2002); doi: 10.1121/1.1492817
View online: http://dx.doi.org/10.1121/1.1492817
View Table of Contents: http://asa.scitation.org/toc/jas/112/2
Published by the Acoustical Society of America

Broadband sound generation by confined turbulent jets

Zhaoyan Zhang, Luc Mongeau,[a] and Steven H. Frankel
School of Mechanical Engineering, Purdue University, West Lafayette, Indiana 47907-1077

(Received 9 November 2001; revised 14 May 2002; accepted 17 May 2002)

Sound generation by confined stationary jets is of interest to the study of voice and speech production, among other applications. The generation of sound by low Mach number, confined, stationary circular jets was investigated. Experiments were performed using a quiet flow supply, muffler-terminated rigid uniform tubes, and acrylic orifice plates. A spectral decomposition method based on a linear source-filter model was used to decompose radiated nondimensional sound pressure spectra measured for various gas mixtures and mean flow velocities into the product of (1) a source spectral distribution function; (2) a function accounting for near field effects and radiation efficiency; and (3) an acoustic frequency response function. The acoustic frequency response function agreed, as expected, with the transfer function between the radiated acoustic pressure at one fixed location and the strength of an equivalent velocity source located at the orifice. The radiation efficiency function indicated a radiation efficiency of the order $(kD)^2$ over the planar wave frequency range and $(kD)^4$ at higher frequencies, where k is the wavenumber and D is the tube cross sectional dimension. This is consistent with theoretical predictions for the planar wave radiation efficiency of quadrupole sources in uniform rigid anechoic tubes. The effects of the Reynolds number, Re, on the source spectral distribution function were found to be insignificant over the range $2000<\mathrm{Re}<20\,000$. The source spectral distribution function approximately obeyed a St^{-3} power law for Strouhal number values $\mathrm{St}<0.9$, and a St^{-5} power law for $\mathrm{St}>2.5$. The influence of a reflective open tube termination on the source function spectral distribution was found to be insignificant, confirming the absence of a feedback mechanism. [DOI: 10.1121/1.1492817]

PACS numbers: 43.70.Aj, 43.28.Ra [MSH]

LIST OF SYMBOLS

a	sphere diameter (m)
c	speed of sound (m/s)
d	orifice diameter (m)
D	tube cross section dimension (m)
f	frequency (Hz)
E	nondimensional sound pressure spectrum
F	source spectral distribution function
g	Green's function
G	acoustic frequency response function
G_{exp}	measured system transfer function
He	Helmholtz number, fD/c
k	wave number (m^{-1})
L	distance from the orifice (m)
M	radiation efficiency function
P	sound power
p	total pressure (Pa)
p'	acoustic pressure (Pa)
r	distance between source and observer (m)
R	reflection coefficient
Re	Reynolds number, Ud/v
S_{pp}	sound pressure spectral density
St	Strouhal number, fD/U
T_{ij}	Lighthill stress tensor
U	jet centerline velocity (m/s)
v_c	velocity of the sphere center (m/s)
x	observer position
y	source position
Δp	mean pressure drop across the orifice (Pa)
ρ_0	ambient density ($\mathrm{kg/m}^3$)
ρ'	acoustic density ($\mathrm{kg/m}^3$)
ω	angular frequency (rad/s)
ν	kinematic viscosity ($\mathrm{m/s}^2$)
σ_{ij}	viscous stress tensor (Pa)
τ	source time coordinate
σ	standard deviation
ϕ	sound source strength

I. INTRODUCTION

Sound generation by jet flows has been the object of many previous investigations (Blake, 1986). Most of these studies have considered the problem of sound production by free high-speed jets because of its importance for aircraft engine noise (Hubbard, 1994). There has been relatively less interest in noise from low-speed confined jets. The motivation for the study described in this paper is the potential significance of this problem for speech production. Sound generation by confined low-speed jet flows is always involved in the generation of fricative consonants, an important component of speech. It may also contribute to voice production, since the jet plume downstream of the glottis is

[a]Author to whom correspondence should be addressed. Electronic mail: mongeau@ecn.purdue.edu

most likely turbulent over a large fraction of one glottis oscillation. Turbulence may be responsible for a random component in the sound produced by the air flow through the larynx, which may play a significant role in defining voice quality. A better understanding of this contribution could help develop better models for speech synthesis, and assist in the diagnosis of pathological voice conditions.

Jet noise theory is usually based on the work of Lighthill (1952), and subsequent refinements by many investigators, in which the basic equations for the fluid motion are formulated in the form of an inhomogeneous wave equation. This approach, termed the acoustic analogy, allows presumed sound source terms to be identified. In particular, for nonheated subsonic free jet flows, the source term is the double divergence of Lighthill's stress tensor, a quantity dominated by the instantaneous, time varying Reynolds stress tensor. In a free field, the source distribution is of a quadrupole-type, known to be an inefficient sound generation mechanism relative to monopole or dipole contributions. The radiated sound pressure may be obtained from the convolution of the source term and a free space Green's function over the entire region where the instantaneous Reynolds stress is significant.

The confinement of the source in a channel modifies the generation and propagation of sound waves significantly. The characteristics of the turbulent jet flow are also different due to the effects of confinement. For example, the strength of the recirculation region is often increased. Additional sources may arise from the impingement of the jet plume on the rigid walls. Finally, the one-dimensional nature of the radiated sound waves at low frequencies changes the basic character of the sound sources from quadrupole- to dipole-, or monopole-type sources. This generally enhances sound production efficiency.

The theory of sound production by turbulence in a rigid pipe has been discussed by Davies and Ffowcs Williams (1968). Lighthill's acoustic analogy was used, with a theoretical expression for the Green's function satisfying rigid boundary conditions on the walls of a rectangular pipe. The radiated sound pressure spectral density was expressed as the summation of acoustic modes within the pipe. A dimensional analysis of the predicted radiated acoustic power was performed. Two limiting cases were considered: (1) low frequencies, where the planar wave mode of propagation dominates; and (2) high frequencies, where higher order duct modes are excited. It was found that the sound power from large-scale turbulence scales with the sixth power of the jet centerline velocity, regardless of frequency. The sound power from small-scale turbulence at low frequencies scales with the sixth power law of the jet velocity. At high frequency (above the cut-on frequency of the first high acoustic mode in the tube), the sound power scales with the eighth power of the jet velocity, similar to the power scaling law of free subsonic jets.

A similar approach was followed by Nelson *et al.* (1981) to study sound production by sound absorbing splitters in a flow duct. The sound source term was modeled as a dipole. The differences in behavior at low and high frequencies were again highlighted. The sound power within the low- and high-frequency regions obeyed a U^4 and a U^6 power law, respectively. Measured sound pressure spectra were cast in nondimensional form. It was shown that one-third octave band sound power spectra measured for various flow speeds were in satisfactory agreement with the postulated scaling laws.

The production of broadband sound from air flow through the larynx, the vocal tract, and the airway has been sparsely investigated (Harper, 2000). In early experiments by Meyer-Eppler (1953), a critical Reynolds number was identified below which there was no significant turbulent sound generation. Meyer-Eppler postulated that the sound pressure increased with the square of the Reynolds number. The contribution of flow impingement on obstructions in the vocal tract was investigated using a hierarchy of physical models by Shadle (1986). The sound pressure generated by flow impingement was found to increase with the third power of the volume flow rate, and decrease with the 2.5th power of the cross-sectional area of the obstruction (Stevens, 1998). Stevens describes the sound spectrum associated with flow impingement as having a broad peak distributed around a certain Strouhal number value, based on the local flow velocity and the duct diameter near the obstruction. Landau and Lifshitz (1997) have estimated that for turbulence in a tube, the roll-on frequency of the sound spectrum is of the order of u/D, and the cutoff frequency is of the order of $u\mathrm{Re}/D$, where u is the flow velocity and D is the diameter of the tube. The recent work of Harper (2000), aimed at a better understanding of breathing sounds, is again based on a Reynolds number power law. Such models neglect the possible influence of frequency on sound production (i.e., Strouhal number effects). The influence of the acoustic response of the cavities and the duct on the power law exponents is based on an inverse filtering approach, which may not yield accurate results when the sound source region is spatially distributed and incoherent.

In confined jet flows, acoustic effects such as sound reflection and resonance are often present. At low frequencies, longitudinal plane acoustic waves may be reflected at the tube termination or at any location where the cross-sectional area changes, setting up standing waves and causing resonance. At high frequencies, where higher order modes are excited, the acoustic field is three-dimensional. The acoustic response of the system then becomes more complicated, with acoustic modes depending on boundary conditions at the tube walls and the termination. These phenomena significantly affect the level and the spectral content of the radiated sound, which makes it difficult to isolate and study the source characteristics directly from sound pressure measurements.

It is desirable to separate the spectral characteristics of the sound source from the acoustic response of the ducting system in order to develop source-filter models that can be utilized over a range of flow conditions, and different working fluids. Weidemann (1971) developed a spectral decomposition method for the separation of source characteristics and system response from experimental data based on acoustic similarity laws for fan noise. The similarity laws express nondimensional radiated sound pressure spectra as the product of a source function, which is presumed to be a function

of only the Strouhal number, and an acoustic frequency response function, presumed to be a unique function of the Helmholtz number. The Mach and Reynolds numbers also appear in the form of power laws. Neise (1975) verified the acoustic similarity laws for the tonal sound emitted by industrial centrifugal fans. Bartenwerfer *et al.* (1976) argued that the source spectral characteristics should be a function of both the Strouhal number and the Reynolds number, and questioned the relevance of power law terms. Mongeau *et al.* (1995) applied the spectral decomposition method to study the aerodynamic sound generating mechanisms in a turbomachinery rotor. The usefulness of the source-filter based method was demonstrated by varying the source characteristics and the acoustic loading independently.

The purpose of the present study was to investigate the characteristics of aerodynamic broadband sound generation by stationary confined jet flows. The ultimate goal is to develop semi-empirical models (scaling laws) that could allow the amplitude and the spectrum of the random component of synthesized voice signals to be established. To accomplish this, the spectral decomposition method was used to isolate source characteristics from other sound propagation effects. Circular orifices were used, as a first step, to investigate the validity and the usefulness of the approach. The effects of orifice geometry are considered in an ongoing, parallel study.

II. SOUND GENERATION BY STATIONARY CONFINED TURBULENT JETS

Consider sound generation by a finite region of turbulence in a long rigid rectangular tube. The tube may or may not be anechoically terminated. Lighthill's equation, which is derived from the continuity and momentum equations, is

$$\frac{\partial^2 \rho'}{\partial \tau^2} - c_0^2 \nabla^2 \rho' = \frac{\partial^2 T_{ij}}{\partial y_i \partial y_j}, \tag{1}$$

where $\rho' = \rho - \rho_0$ is the fluctuating density, and $T_{ij} = \rho u_i u_j + \delta_{ij}(p - c_0^2 \rho') - \sigma_{ij}$ is Lighthill's stress tensor. The corresponding inhomogeneous Helmholtz equation is, with $p' = c_0^2 \rho'$,

$$\left(\frac{\partial^2}{\partial y_i^2} + k_0^2 \right) p'(y,\omega) = -\phi(y,\omega), \tag{2}$$

where $k_0 = \omega/c$ is the wave number, and $\phi(y,\omega) = \partial^2 T_{ij}(y,\omega)/\partial y_i \partial y_j$ is the Fourier transform of the sound source term. Variables with ω as a parameter are the Fourier transform of their time domain counterparts.

To solve Eq. (2), the normal velocity is assumed to vanish on the walls. From the momentum equation, neglecting viscous drag forces on the walls, this boundary condition corresponds to the vanishing of the normal pressure gradient. Equation (2) may be solved by means of a Green's function defined as the solution of

$$\left(\frac{\partial^2}{\partial y_i^2} + k_0^2 \right) g(x,y;\omega) = -\delta(x-y) \tag{3}$$

with the boundary condition $\partial g/\partial n|_{\text{wall}} = 0$ on the wall, as well as additional boundary conditions at the tube ends for finite length tubes. The coordinates x and y are the observer and source location, respectively. Note that the Green's function defined here accounts for both the impedance and the geometry of the boundary. Multiplying Eq. (2) by $g(x,y;\omega)$, subtracting the product of Eq. (3) and $p'(y,\omega)$, and integrating with respect to y over the whole flow region yields, after applying the divergence theorem and the boundary conditions,

$$p'(x,\omega) = \int_V g(x,y;\omega)\phi(y,\omega)dV(y). \tag{4}$$

Note that the neglection of the viscous drag on the orifice walls is probably justified. A parallel computational study of a similar flow in a rigid duct (Zhao *et al.*, 2001) showed that the viscous drag component of the dipole sound is very small compared with the pressure drag component.

In the case of an observer far from the source region, the distance between the observer and the source location is much larger than the extent of the source region. Then time retardation effects between the source and observer due to source motion can be neglected. Therefore, the Green's function can be expressed as the product of two terms as follows:

$$g(x,y;\omega) = g_x(x,\omega) g_y(y,\omega). \tag{5}$$

The far-field term, g_x, accounts for sound propagation from immediately outside the source region to the observer, therefore representing the acoustic response of the system. The near field part of the Green's function, g_y, reflects the radiation efficiency of the sound generation processes described by the source term $\phi(y,\omega)$.

The sound pressure spectral density S_{pp} and the cross-spectral density of the source term $S_{\phi\phi}$ are defined here as

$$S_{pp}(x,\omega) = \lim_{T\to\infty} \frac{2\pi}{T} \{p'(x,\omega) p'^*(x,\omega)\}, \tag{6}$$

$$S_{\phi\phi}(y_1,y_2;\omega) = \lim_{T\to\infty} \frac{2\pi}{T} \{\phi(y_1,\omega)\phi^*(y_2,\omega)\}. \tag{7}$$

From Eqs. (4) and (5), the sound pressure spectral density is related to the source cross-spectral density through

$$S_{pp}(x,\omega) = |g_x(x,\omega)|^2 \int_V \int_V S_{\phi\phi}(y_1,y_2;\omega) g_y(y_1,\omega) \times g_y(y_2,\omega) dV(y_1) dV(y_2). \tag{8}$$

According to the principle of superposition in linear acoustics, the sound pressure radiated by a distribution of sound sources is the sum of the sound pressures generated by each elemental source within the distributed source region. Radiation enhancement or cancellation occurs depending on time or phase retardation effects. These depend on the distance between the source and observer, as well as the spatial and phase distribution of the distributed sources. These interferences are described by the convolution integral in Eq. (4). For a far-field observer, the effect of varying the source-observer distance on sound waves' superposition can be separated from retarded time effects. In other words, the far-

field part of the Green's function may be moved outside the integral, as shown in Eq. (8).

For a compact source distribution, the turbulence length scale of the source is much smaller than the wavelength typical of the sound radiation so that the effect of the spatial and phase distribution of the source is insignificant and can be ignored. The parameter kD is much smaller than unity, where $k=\omega/c$ is the wave number and D is the typical length scale of the source distribution. Large scale of turbulence contributes the most to the radiated sound field, and so the length scale D is comparable to a typical tube dimension (width or height). The convolution then becomes a simple summation, instead of a summation at the retarded time. For a multipole source of order n, this integral is of the order of $(kD)^{2n}F^2$ (Howe, 1998), where F is the typical value of the source strength. The $(kD)^{2n}$ term is a measure of the so-called radiation efficiency, which is defined as the ratio of the radiated sound power to the mechanical power driving the sound generation phenomena. The radiation efficiency decreases with ascending multipole order.

The far-field sound spectra in Eq. (8) can be reorganized as the product of a source spectral function, a radiation efficiency function, and a far-field term. As discussed before, the far-field term describes the effects of sound propagation phenomena from the source region to the observer. It may be construed as the frequency response function between the Thevenin equivalent source strength (see, for example, Flanagan, 1965) and the sound pressure radiated at the observer position. The radiation efficiency, on the other hand, is a measure of sound production. It is straightforward, then, to express the nondimensional sound pressure spectrum, $E=S_{pp}(x,f)/(\frac{1}{2}\rho U^2)^2 d/U$, as

$$E=F(d,D,f,U,\upsilon)M(kD)G(x,D,f,c,R). \tag{9}$$

The sound pressure spectral density, S_{pp}, has the dimensions of pressure^2/frequency and is made nondimensional using the scaling factor $(\frac{1}{2}\rho U^2)^2 d/U$. The function F is the source spectral distribution function, the function G is the system transfer function or response function term, and M is a radiation efficiency function which depends on (kD).

The source function F depends on flow parameters such as the centerline velocity of the jet, U, the tube cross-sectional dimension, D, the orifice diameter, d, the fluid viscosity υ, as well as frequency, f. The system frequency response, G, depends on the observer position, x, the tube dimension, D, the speed of sound, c, and the acoustic boundary conditions, R. Defining the dimensionless groupings $\mathrm{Re}=Ud/\nu$, $\mathrm{St}=fD/U$, $\mathrm{He}=fD/c$, the above equation may be rewritten as

$$E=F\left(\mathrm{St},\mathrm{Re},\frac{d}{D}\right)M(\mathrm{He})G\left(\mathrm{He},\frac{x}{D},R\right). \tag{10}$$

The M function and the G function can be combined to form a new function G_1:

$$G_1\left(\mathrm{He},\frac{x}{D},R\right)=M(\mathrm{He})\cdot G\left(\mathrm{He},\frac{x}{D},R\right). \tag{11}$$

Substituting back into Eq. (10) yields the simple nondimensional source-filter form:

$$E=F\left(\mathrm{St},\mathrm{Re},\frac{d}{D}\right)G_1\left(\mathrm{He},\frac{x}{D},R\right). \tag{12}$$

III. EXPERIMENTAL APPARATUS

The experimental apparatus was a slightly modified version of an apparatus used in a parallel voice production study (Zhang *et al.*, 2002). A circular orifice plate was installed between two rectangular tubes, as illustrated in Fig. 1(a). Each tube had a square cross-section, 2.25×2.25 cm, and was 22.5 cm long. The geometry of the orifice is shown in Fig. 2. The circular orifices featured a converging nozzle at the entrance and a sharp trailing edge. Two orifice diameters, 0.381 and 0.635 cm, were used. Acoustically treated terminations were connected to each test section to reduce possible sound reflections. The terminations consisted of two corrugated, rubber hoses with different inner diameters. The smaller hose, with a 2.54-cm i.d., was connected directly to the rectangular tube at one end. At the other end, the smaller hose was perforated and wrapped using Fiberglass over a 1-m-long section. This end section was then inserted into a larger rubber hose with a 5.08-cm i.d. The junction was sealed to avoid any flow leakage.

The flow supply allowed for the use of different gas mixtures [Fig. 1(b)] in the experiments. Use of different working fluids makes it possible to study the possible dependence of sound generation on fluid properties. A helium–CO_2 mixture was used because it allowed the speed of sound and viscosity to be varied over a large range. The two gases were fed into a mixing tank, and then into the test sections. A mass flow controller (MKS Type 1559A) on each branch of the inlet gases was used to maintain the desired composition as well as the total flow rate. A third port allowed pressurized air to be delivered to the mixing tank through a switch valve. This made it possible to use either helium–CO_2 mixtures or air. A thermocouple was installed in the outlet to measure the mixture temperature, from which the density of the mixture was calculated. To reduce possible noise from the flow supply, the mixing tank walls were lined with a 2.54-cm-thick layer of Fiberglass.

Radiated sound pressure spectra were measured using two microphones (6.35-mm diameter, B&K 4938) located 14 cm upstream and downstream from the orifice plate. The volumetric flow rate through the orifice was measured using a precision mass-flow meter (Baratron type 558A) at the inlet of the test section. The time-averaged pressured gradient across the orifice was measured using a pressure gauge (Baratron type 220C). The output signals from the microphones were acquired at a sampling rate of 32 768 Hz using an HP356XA data acquisition system.

IV. EXPERIMENTAL RESULTS

The sound pressure spectra radiated downstream were measured for different flow rates, and two different orifice diameters. The jet centerline velocity was calculated using Bernoulli's equation:

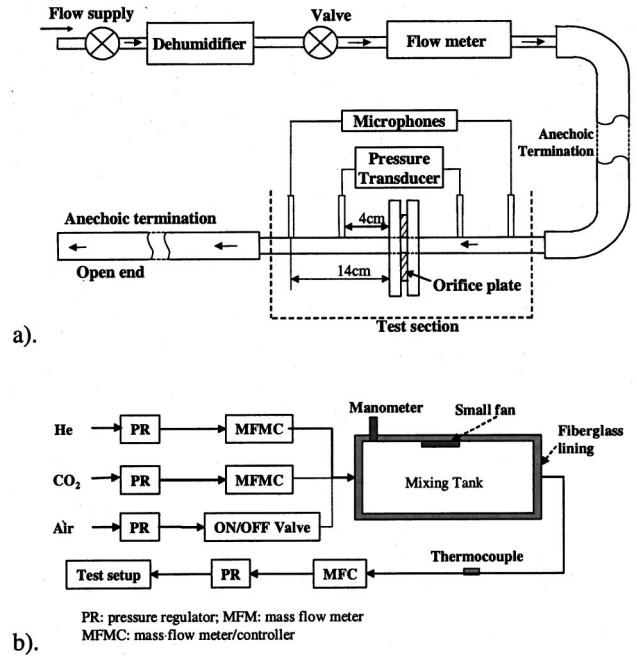

FIG. 1. (a) Schematic of the experimental apparatus. (b) Flow supply system.

$$U=\sqrt{2\Delta p/\rho_0}, \tag{13}$$

where Δp is the pressure drop across the orifice and ρ_0 is the medium density. Three different helium–CO_2 mixtures, with helium mole ratios of 0, 0.33, and 0.57, were used, as well as air.

Figure 3 shows radiated sound spectral densities, S_{pp}, measured downstream for air, several flow rates, and for the 0.381-cm-diam orifice. The spectral levels, as expected, increase as the flow rate, or jet velocity, increases. The high

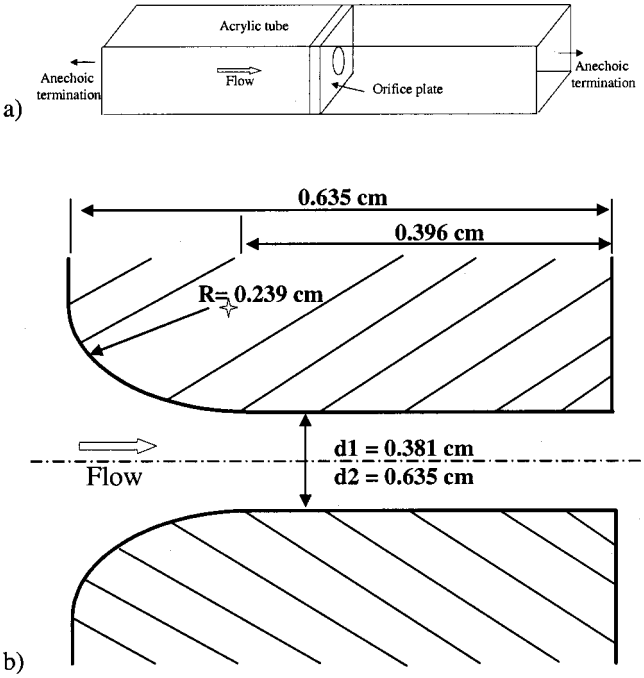

FIG. 2. (a) Test section. (b) Cross section of the circular orifices. Dimensions in cm.

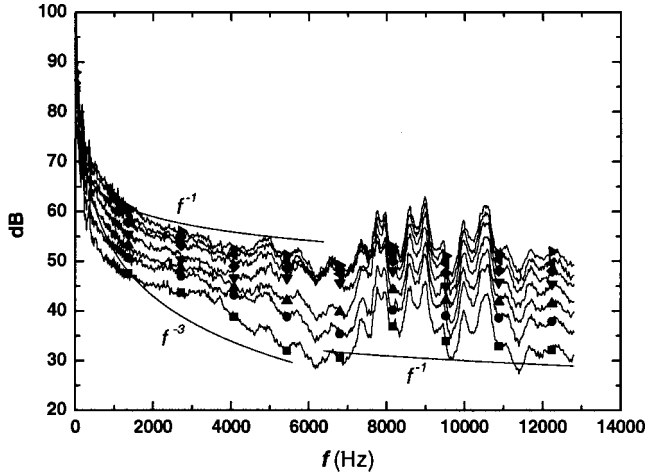

FIG. 3. Downstream sound pressure spectra for different orifice static pressure drops, $d=0.381$ cm, air is the medium. ■: $\Delta p=6$ cm H_2O; ●: $\Delta p=8$ cm H_2O; ▲: $\Delta p=10$ cm H_2O; ▼: $\Delta p=12$ cm H_2O; ♦: $\Delta p=14$ cm H_2O; ◀: $\Delta p=16$ cm H_2O; ▶: $\Delta p=18$ cm H_2O.

sound pressure levels at very low frequencies are believed to be due to flow supply noise. The effectiveness of the anechoic terminations is reduced at low frequencies, causing resonance (below 500 Hz).

Efforts were first made to establish power laws based on the jet velocity to collapse the sound spectral data. Different scaling laws work best at low frequencies and at high frequencies. At frequencies lower than the high mode cut-on frequency (approximately 7000 Hz for the rectangular tube), the spectra collapse when scaled using U^6, while at frequencies higher than the cutoff frequency, the spectra collapse using a U^8 law. Similar scaling laws for jet velocity were obtained for other mixtures, although the optimal value of the exponents varied slightly for different flow conditions.

The sound spectral level was observed to increase with the orifice diameter, as shown in Fig. 4. Different power laws for the dependence on jet diameter were also found for low frequencies and high frequencies. The low frequency components collapse very well when scaled with d^2. The high frequency components collapse better when scaled with d,

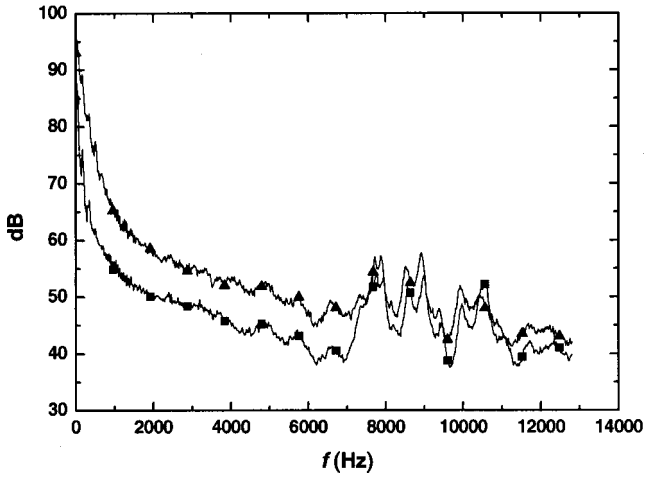

FIG. 4. Downstream sound pressure spectra for different orifice diameters, $\Delta p=10$ cm H_2O, air is the medium. ■: $d=0.381$ cm diameter; ▲: $d=0.635$ cm diameter.

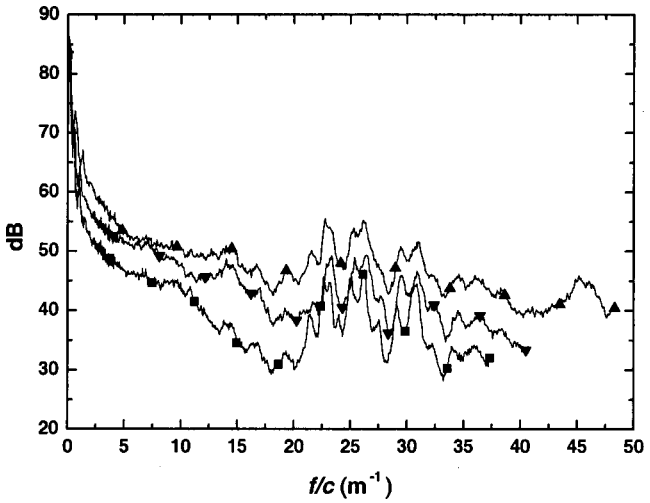

FIG. 5. Downstream sound pressure spectra for different media, and speed of sound, $d=0.381$ cm, $U=31.3$ m/s. ■: $c=343$ m/s; ▼: $c=316$ m/s; ▲: $c=268$ m/s.

with the optimal value of the exponent lying between 1 and 2. The diameter exponent also varied slightly with the flow conditions.

Figure 5 shows radiated sound spectra for different gas mixtures. Generally, the sound level is observed to increase as the speed of sound is decreased. The sound spectra were found to collapse best when scaled using a $c^{-2}\rho^2$ power law. As for the previous cases, such power scaling law does not work well at all frequencies.

To find the optimal value of the power law exponents (assuming the sound power is proportional to $U^m d^n$) as a function of frequency, the spectra were integrated from a starting frequency f_2 up to the upper limit frequency of 12.8 kHz. Figure 6 shows the exponents m, n as a function of the integration starting frequency f_s. For $f_s<300$ Hz, m decreases towards 3 due to the presence of strong flow supply noise at very low frequency. Above 8 kHz, m tends towards a value of 8. Between 300 and 8000 Hz, m is around 7. These values are consistent with the observations of Davies and Ffowcs Williams (1968). The diameter exponent, n, decreases with frequency until it approaches a value near unity above 5 kHz. It is clear that a simple power law formulation

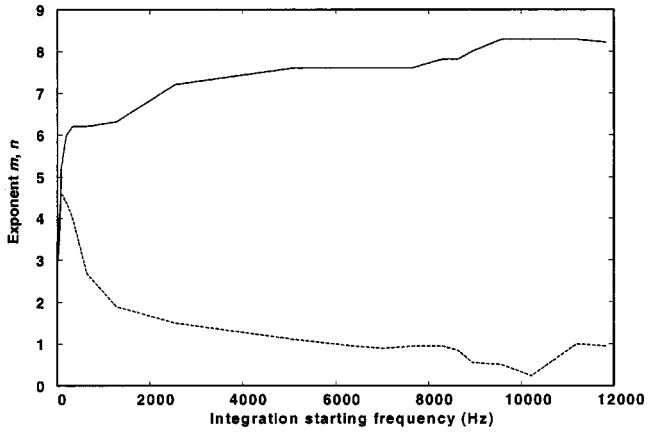

FIG. 6. Frequency dependence of the exponents in the sound power laws $P\sim U^m d^n$. ———: m; - - -: n.

is not sufficient to accurately predict the effects of flow velocity or orifice diameter. The spectral distribution of the sound spectra must be considered in the analysis.

V. SPECTRAL DECOMPOSITION PROCEDURE

The spectral decomposition method assumes a linear source-filter system, with the sound generated by the turbulent jet through the orifice acting as the source, and the filter related to the acoustic response of the system. The output signal is the measured radiated sound pressure. It is assumed that there is little or no feedback, or back reaction of the flow to the radiated sound field.

Expressing the nondimensional spectrum using a logarithmic scale, Eq. (12) is rewritten as

$$10\log E = 10\log F\left(\mathrm{St},\mathrm{Re},\frac{d}{D}\right)+10\log G_1\left(\mathrm{He},\frac{x}{D},R\right). \tag{14}$$

For a fixed microphone position, constant acoustic boundary conditions and orifice diameter, G_1 is a function of only the He number. Removing the d/D, x/D, and R dependence, Eq. (14) becomes

$$10\log F(\mathrm{St},\mathrm{Re}) = 10\log E - 10\log G_1(\mathrm{He}). \tag{15}$$

Nondimensional sound spectra may be plotted against the St number and the Re number for values of f and c forming a constant He number. Since no coupling is assumed between the F and G_1 functions, surfaces of constant He number should be parallel to each other. They would have the same functional shape and only differ by a nearly constant level difference over the St-Re plane. This level difference, according to Eq. (15), is the value of $10\log G_1$. The spectral surfaces He=const can be interpolated from the available data points. By calculating the level difference between the spectral surfaces He=const, using a least squares method, the relative amplitude of G_1 values can be determined. This process can be tentatively formulated:

$$10\log G_1(\mathrm{He}_2)-10\log G_1(\mathrm{He}_1) = \overline{10\log[F\times G_1](\mathrm{He}_2)-10\log[F\times G_1](\mathrm{He}_2)}, \tag{16}$$

where the overbar means an ensemble average of all data available for the discrete He_1 and He_2 values. Arbitrarily imposing $G_1(\mathrm{He}_{\min})=0$, where $\mathrm{He}_{\min}$ is minimum value of the He number in the experimental data, the G_1 function can then be uniquely constructed by repeating the same procedure over the entire range of He. This allows $10\log F^k$ functions to be obtained for each combination of the Strouhal number and the Reynolds number using Eq. (15). Finally, the function $10\log F$ is obtained by ensemble-averaging all $10\log F^k$ functions.

Two test cases were used to verify the decomposition method, as described below.

A. Accuracy of the spectral decomposition method

Explicit analytical expressions for the F and G_1 functions were used to generate calculated ''data'' in a simulated ''experiment,'' this to study the accuracy of the method. The F and G_1 function were arbitrarily chosen as

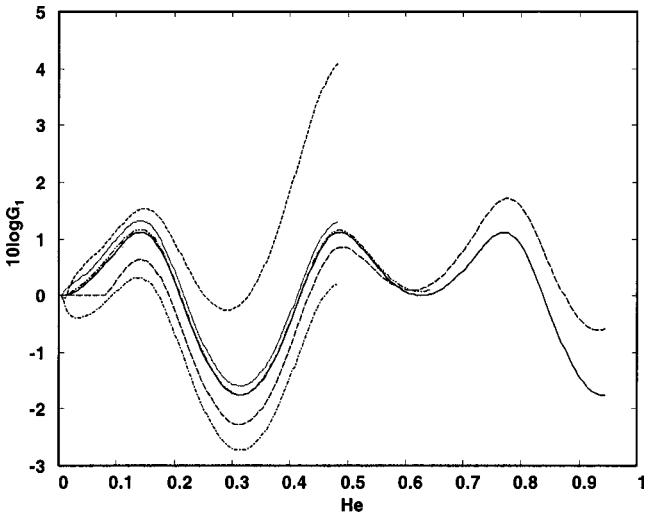

FIG. 7. Comparison between the correct and the estimated values of the G function, and constructed values obtained using spectral decomposition. The accuracy of the decomposition increases as the input spectra overlap in the St-Re plane is increased. ———: exact solution; – –: case Ia; - - -: case Ib; —·—·—·—: case II; –··–: case III; · · · ·: case IV.

$$F=\mathrm{Re}^{0.2}(\mathrm{St}^2+10), \quad G_1=\left|\frac{e^{5j\mathrm{He}}+0.2e^{-5j\mathrm{He}}}{e^{10j\mathrm{He}}+0.2e^{-10j\mathrm{He}}}\right|. \tag{17}$$

The nondimensional spectra E were then constructed based on Eq. (14). To simulate the experiments, the sound spectra S_{pp} were constructed for six different values of velocity and four values of speed of sound (or four different media), with a frequency resolution bandwidth of 16 Hz.

To test the accuracy of the decomposition method, four different spectral data sets were used as input to the decomposition program. Spectra constructed from 1, 2, 3, and 4 different values of speed of sound were used in cases I, II, III, and IV, respectively. It was found that the accuracy of the reconstructed functions depends highly on the distribution and the size of overlap region of the data sets over the St-Re plane. For a constant He number, the data set constructed for one discrete value of speed of sound maps to a hyperbolic curve in the St-Re plane. One curve in the St-Re plane is certainly not enough for accurate interpolation of the He =const surface for the 10log$E$ function over the whole St-Re plane, and errors in the interpolation process could lead to errors in calculation of the 10logG_1 function. Figure 7 shows the reconstructed G_1 functions for all four cases along with the exact solution, Eq. (17). Case I, using spectra constructed for two discrete values of the speed of sound (cases Ia and Ib), resulted in a biased estimate, with an accumulated error in excess of 3 dB over a reasonable range of He numbers. This bias gradually disappeared as more and more data sets were used, increasing the number of curves available for surface interpolation as well as the overlap (or redundancy) in the data set. For case III, in which spectra were constructed using three different values of speed of sound, the reconstructed G_1 function matched very well the exact solution. Case IV also yielded a very good agreement, except for a constant offset due to the arbitrary selection of the value of G_1 at $\mathrm{He}_{\min}$.

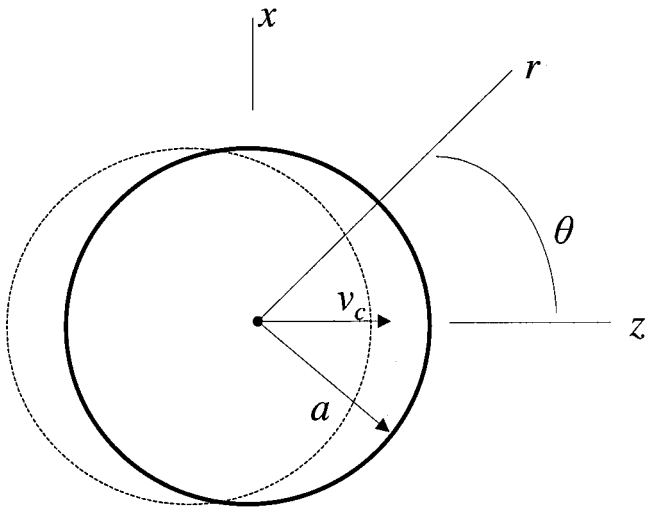

FIG. 8. Transversely oscillating rigid sphere in free space.

B. Transversely oscillating rigid sphere in free space

Next, the simple problem of sound radiation from a transversely oscillating rigid sphere in free space was used to illustrate the application of the similarity laws formulation. Consider, as illustrated in Fig. 8, the center of a rigid sphere with radius a oscillating along the z-axis about the origin with a velocity $v_c(t)=\mathrm{Real}(\hat{v}_c e^{-iwt})$, where $\hat{v}_c$ is the complex velocity. This is a classical example of a dipole sound source. The complex sound pressure at a point at a distance r from the origin along the z-axis is (Pierce, 1989)

$$\hat{p}=\frac{-i\omega\rho}{r^2}\frac{\hat{v}_c a^3 e^{-ika}}{2-(ka)^2-2ika}e^{ikr}(ikr-1). \tag{18}$$

Assuming a compact source, and when the observer is in the far field,

$$\hat{p}=(ka)^2\frac{a}{r}\frac{\rho c\hat{v}_c}{2}e^{ik(r-a)}. \tag{19}$$

In the hydrodynamic near field ($kr\ll 1, r\sim a$), the sound pressure is approximately

$$\hat{p}\approx -i(ka)\frac{\rho c\hat{v}_c}{2}e^{ik(r-a)}. \tag{20}$$

The radiation efficiency, which is the ratio of the far-field sound pressure and the sound pressure in the hydrodynamic near field, is

$$\left|\frac{\hat{p}_{\mathrm{far}}}{\hat{p}_{\mathrm{near}}}\right|^2\approx(ka)^2. \tag{21}$$

Now assume the sphere center velocity time history has a spectrum with spectral components at St numbers which are multiples of a fundamental St_0. The magnitude of each component is assumed to be proportional to the St number:

$$v_c(f)=U\sum_{n=1}^{f_n<f_s/2}\mathrm{St}\cdot\delta(f-f_n), \tag{22}$$

where $f_n=n\cdot\mathrm{St}_0U/a$, f_s is the sampling rate, and U is a constant proportionality factor playing a role similar to that

of velocity in a flow-excited sound problem. The Strouhal number may then be chosen as $\mathrm{St}=fa/U$. The complex sound pressure in the far field then becomes

$$\hat{p}(f)=U\sum_{n=1}^{f_n<f_s/2}\mathrm{St}^2\frac{a}{r}\frac{\rho c}{2}e^{ik(r-a)}\delta(f-f_n), \tag{23}$$

where the wave number $k=f/c$.

Sound power spectra can be constructed from Eq. (23) for different values of U and the speed of sound. Because the complex pressure in Eq. (23) has the dimension of ''pressure'' instead of ''pressure/frequency,'' the nondimensional spectrum is

$$E=\frac{S_{pp}(x,f)}{(\frac{1}{2}\rho U^2)^2}. \tag{24}$$

In this case study, six values of ''velocity'' U and three values of speed of sound were used to construct the sound spectra. The value of St_0 was chosen to be very small so that the spectra were broadbandlike and the spectral data set had significant overlap in the St-Re plane.

For this particular case, the Green's function is the three-dimensional free-space Green's function. For a fixed observer position in the far field of a compact source, this indicates a uniform acoustic response function at all frequencies. The radiation efficiency function M, shown in Eq. (21), is of the order of $(ka)^2$. Therefore, the G_1 function in this case, as defined in Eq. (11), is simply

$$G_1(\mathrm{He})\approx(\mathrm{He})^2. \tag{25}$$

Figure 9(a) shows a comparison between the reconstructed G_1 function and Eq. (25). The two G_1 functions are in very good agreement. The reconstructed and exact source spectral distribution functions F are shown in Fig. 9(b). As prescribed in Eq. (22), the source strength depends linearly on the St number, and thus the spectra should follow a St^2 law. A St^4 dependence is obtained instead, as shown in Fig. 9(b). The additional St^2 dependence is a consequence of the similarity laws formulation. In Eq. (24), the spectra were nondimensionalized by a factor $\frac{1}{2}\rho U^2$, which is the hydrodynamic energy in the near field. Not all of this energy is converted into acoustic power. Only the energy associated with the dilatation component of the velocity field is radiated to the far field. This conversion efficiency is St^2 for a compact source, which can be shown as follows:

$$\left(\frac{|\hat{p}_{\mathrm{near}}|}{1/2\rho U^2}\right)^2\approx\left(\frac{1/2ka\rho cU}{1/2\rho U^2}\right)^2=\left(\frac{kac}{U}\right)^2=\mathrm{St}^2. \tag{26}$$

Taking this into account then yields the observed St^4 trend of Fig. 9(b).

For a confined environment, the near-field flow-acoustic interaction is much more complicated due to the presence of solid surfaces. However, it is expected that the same formulation should also be valid for far-field measurements and compact sources.

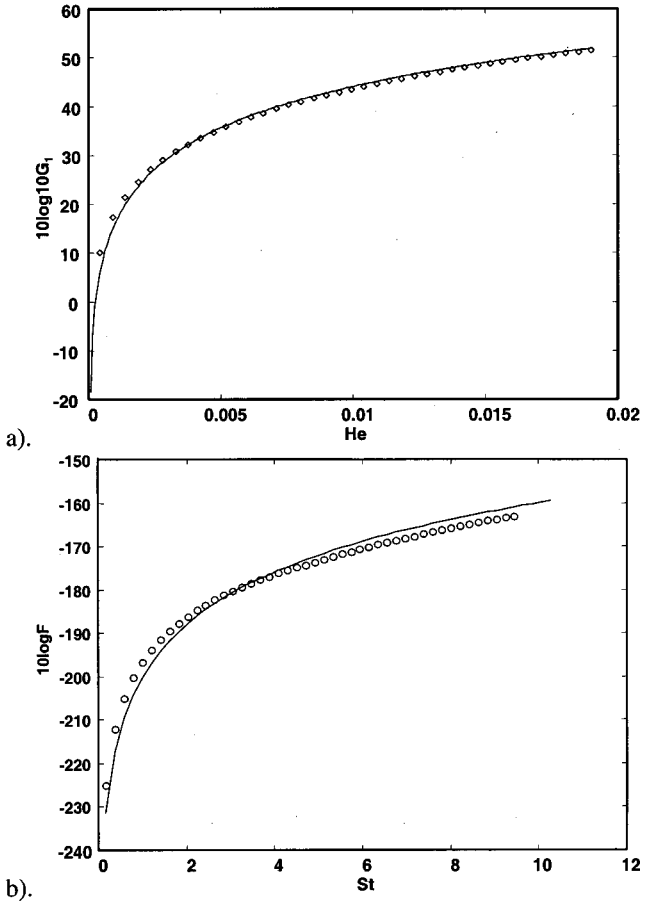

FIG. 9. (a) Comparison between the correct G_1 function, and estimated values obtained using spectral decomposition procedures. ———: 20logHe; ◇: $10\log G_1$. (b) Comparison between the correct F function, and estimated values obtained using spectral decomposition procedures. ———: 40logSt: ○: $10\log F$.

VI. RESULTS, ANALYSIS AND DISCUSSION

The sound spectra measured for varying gas mixtures, orifice diameters, and flow rates, shown in Figs. 3–5, were used to attempt the reconstruction of the source function for radiation by subsonic confined jets. Figure 10 shows nondimensional spectra $10\log E$ for two discrete values of the He

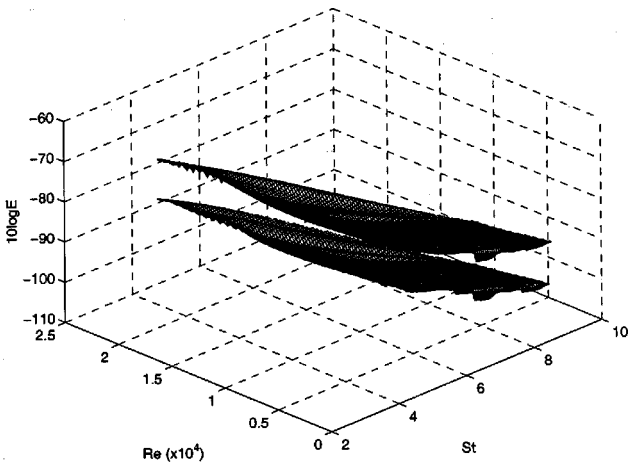

FIG. 10. The nondimensional spectra E for two consecutive He numbers. The two spectral surfaces are parallel to each other. $d=0.635$ cm.

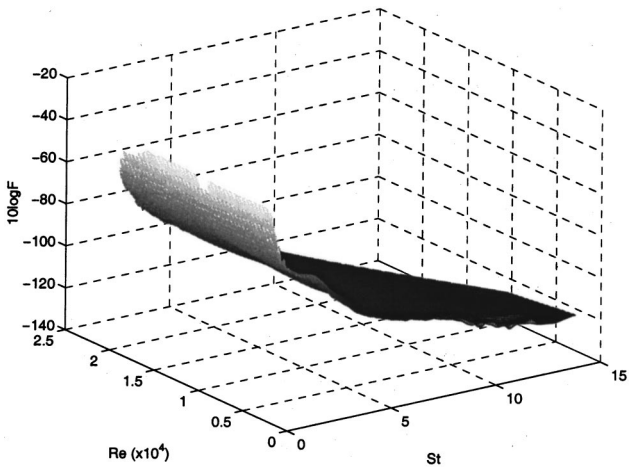

FIG. 11. Averaged source spectral distribution function F. $d=0.635$ cm.

number. For visual convenience, one of the spectral surfaces was offset by 10 dB. The two spectral surfaces are parallel to each other, which supports the validity of the similarity law formulation.

The $10\log G_1$ function was obtained by calculating the difference between neighboring spectral surfaces. The $10\log F$ functions were then obtained by subtracting the known $10\log G_1$ function from the nondimensional spectra $10\log E$. The resulting $10\log F^k$ functions collapsed very well, which is another indication of the validity of the similarity formulation. The ensemble-averaged $10\log F$ function is shown in Fig. 11. The corresponding standard deviation of $10\log F$, shown in Fig. 12, is less than 2 dB. This confirmed the validity of the product law formulation within approximately 1 dB.

Note that the sound pressure spectra were measured at one fixed location along the tube wall. At very low frequency, the microphone may have been in the acoustic near field, as the acoustic wavelength becomes large. Vortices shed from the orifice and/or turbulence may not have been dissipated, and may have caused ''pseudo-sound'' recorded by the microphone. The influence of the near field may have

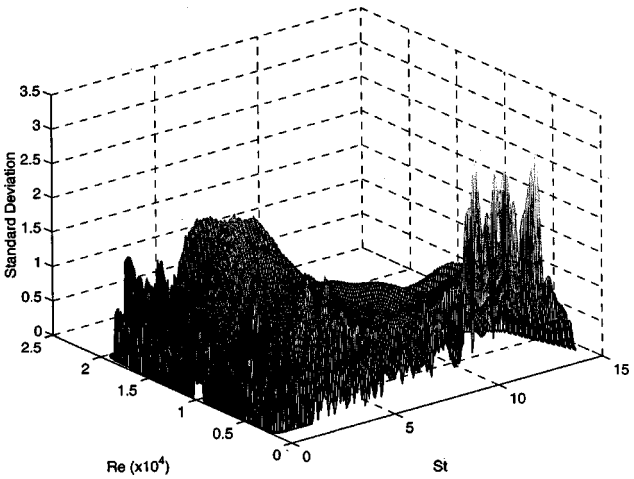

FIG. 12. Standard deviation of the estimated source functions. $d=0.635$ cm.

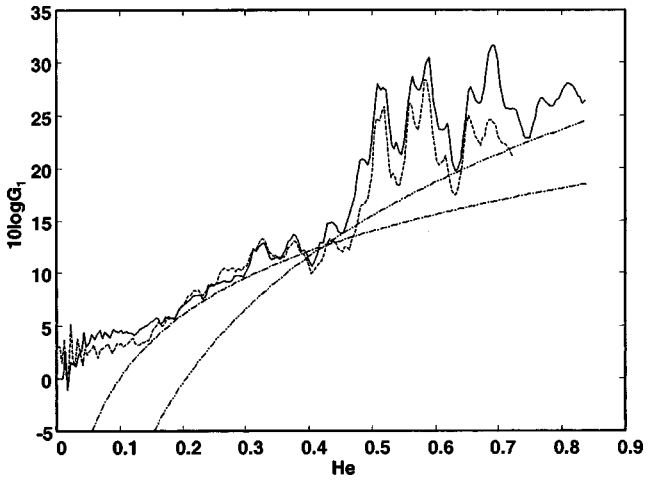

FIG. 13. The G_1 functions obtained for two orifice diameters. ———: $d=0.381$ cm; — — —: $d=0.635$ cm; —·—·—·—: 20logHe; –··–: 40logHe.

colored the radiation efficiency function (or M function) at low frequencies.

A. System response function and radiation efficiency

The acoustic frequency response functions, G_1, obtained for two different orifice diameters are shown in Fig. 13. They are nearly identical. Additional maps showing He^2 and He^4 power laws are also shown in the figure for comparison. These describe approximately the behavior of the G_1 functions at low He numbers and high He numbers, respectively.

As indicated in Eq. (11), the G_1 function is composed of the system frequency response function, G, and the radiation efficiency function, M. The acoustic response function G, as discussed before, can be calculated as the ratio of the sound pressure measured at the microphone position and that which would be measured at the orifice plate location if the tube was not there. Assume planar wave propagation in the tube, as illustrated in Fig. 14. The sound source is located on the left side of the tube, and the tube is terminated by acoustic impedance Z on the right end. With an incidence sound wave of frequency f, the complex sound pressure at the microphone location is

$$\hat{p}_{\mathrm{mic}}(l,f)=A(e^{-ikl}+R\cdot e^{ikl}), \tag{27}$$

where A is the amplitude of the incident wave, $k=2\pi f/c$ is the wave number, and R is the reflection factor which is

$$R=\frac{Z-\rho_0 c_0}{Z+\rho_0 c_0}. \tag{28}$$

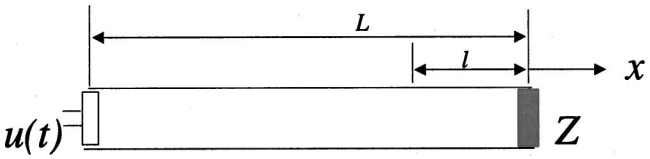

FIG. 14. Schematic of a tube with a velocity type source at one end and terminated with an acoustic impedance.

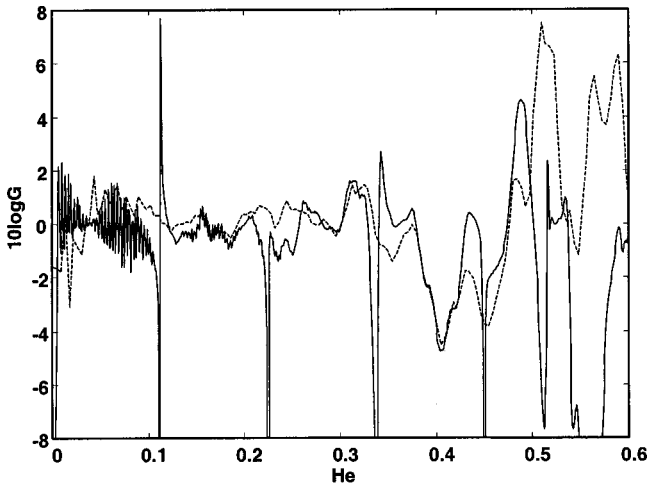

FIG. 15. Comparison between the system acoustic transfer function and the G function. ———: system acoustic transfer function; — — —: 10log$G$.

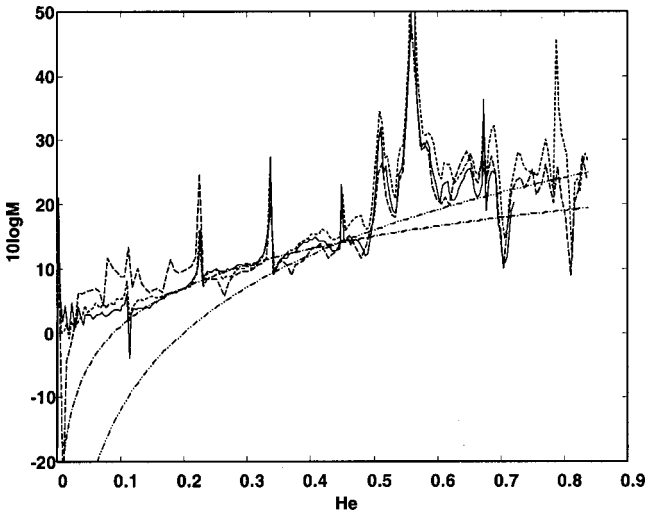

FIG. 16. The radiation efficiency functions obtained for different orifice diameters and downstream tube terminations. ———: $d=0.635$ cm, with anechoic termination; - - -: $d=0.381$ cm, with anechoic termination; — —; $d=0.381$ cm, with finite length tube downstream: —·—·—·—: 20logHe; –···–: 40logHe.

Assuming a velocity type of sound source, the complex sound pressure that would be measured at the source location if the tube was not there is

$$\hat{p}_{\text{source}}(L,f)=A(e^{-ikL}-R\cdot e^{ikL}). \tag{29}$$

The G function is then the ratio of the two complex pressures:

$$G_{\text{exp}}=\left|\frac{A(e^{-ikl}+R\cdot e^{ikl})}{A(e^{-ikL}-R\cdot e^{ikL})}\right|^2=\left|\frac{e^{-ikl}+R\cdot e^{ikl}}{e^{-ikL}-R\cdot e^{ikL}}\right|^2. \tag{30}$$

The notation G_{exp} is used here instead of G to indicate that this response function is obtained experimentally.

The termination impedance was measured using the two-microphone method (Seybert, 1977). The G_{exp} function was then calculated using Eq. (30) and shown in Fig. 15. It is possible to compare functions G_{exp} and G, the latter a component of G_1. The radiation efficiency function was extracted from the G_1 function by matching G with G_{exp}. The result is shown in Fig. 15 together with the G_{exp} function for comparison. There is generally a good agreement, except at frequencies where a pressure node coincides with the microphone location, because of flow noise. Flow noise tends to limit the dynamic range of the G function. The sharp peaks in G_{exp} are most probably due to numerical errors in the calculation of the reflection factor. Discrepancies at high frequencies are likely caused by the excitation of higher order acoustic modes.

To a good approximation, the M function can be determined by regression, as shown in Fig. 13. The mismatch at very low frequencies is, as discussed above, due to the sound pressure measurement in the acoustic near field, although there could be other sources of errors. The M function can also be obtained by subtracting the G_{exp} function from the G_1 function. This is plotted in Fig. 16. The M function approaches He^2 and He^4 for low He numbers and high He numbers, respectively. These trends are in good agreement with the theoretical radiation efficiency of quadrupole sources in tubes. The value of the He number corresponding to the cut-on frequency of higher modes in the test section was about 0.45. At greater He numbers, again, higher order modes are excited and the calculated G_{exp} function is not accurate. The agreement between the He^4 regression and the reconstructed M function is not as good.

There are two major sound sources in sound radiation from confined stationary jets: quadrupole sources due to the turbulence region downstream the orifice and dipole sources due to the unsteady force applied to the fluid by the downstream wall of the orifice (Zhang *et al.*, 2002). The quadrupolelike radiation efficiency obtained in this study indicates that the dipole sources contributions may have been negligible in the present case. The flow within the orifice may have been laminar or very stable, so that the fluctuating axial force induced by the interaction between the orifice wall and the flow was very small.

B. Source spectral distribution function

Figure 17 shows the source spectral function (also shown in Fig. 11) versus Reynolds number for constant

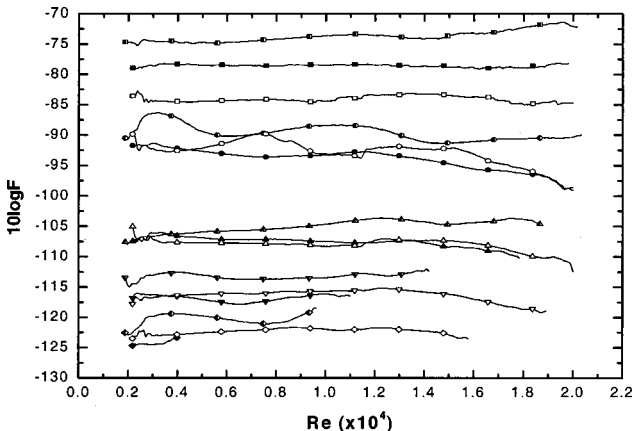

FIG. 17. The source distribution function F as a function of Reynolds number for constant Strouhal number. ■: St=1; ●: St=3; ▲: St=6; ▼: St=9; ♦: St=12. Solid symbols: $d=0.381$ cm, with anechoic termination; open symbols: $d=0.381$ cm, finite-length tube; half open symbols: $d=0.635$ cm, with anechoic termination.

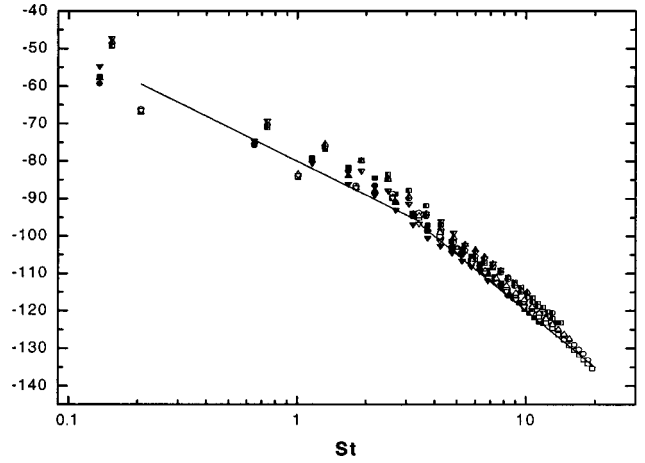

FIG. 18. The source distribution function F as a function of Strouhal number for constant Reynolds numbers. ■: $\mathrm{Re}=0.4\times10^4$; ●: $\mathrm{Re}=0.8\times10^4$; ▲: $\mathrm{Re}=1.2\times10^4R$; ▼: $\mathrm{Re}=1.6\times10^4$. Solid symbols: $d=0.381$ cm, with anechoic termination; open symbols: $d=0.381$ cm, finite-length tube; half open symbols: $d=0.635$ cm, with anechoic termination. ———: two-segment curve.

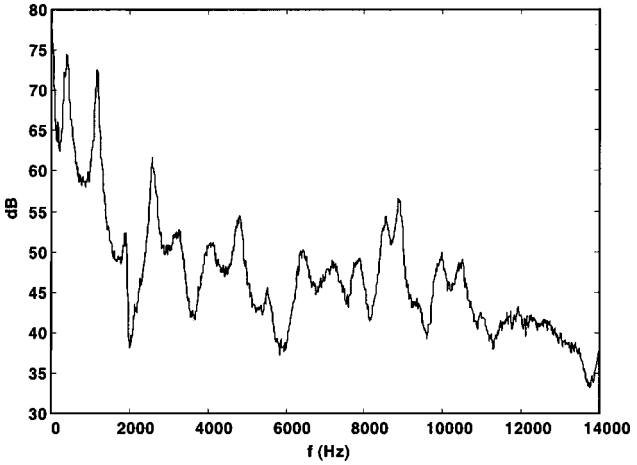

FIG. 19. Downstream sound pressure spectrum for the case with finite length tube downstream of the orifice plate. $d=0.381$ cm, $\Delta p=12$ H_2O, and air.

Strouhal number. The Reynolds number influence was nearly negligible over the range considered (2000 to 20 000), though a very progressively slow increase in the source amplitude with the Reynolds number was observed. The F function obtained for the larger orifice diameter (0.635 cm) was approximately 2 or 3 dB higher in level than the F function obtained for the smaller orifice diameter (0.318 cm). This difference decreased slightly as the St number increased, indicating a dependence on d at low values of St, which is consistent with the d^2 low-frequency scaling law discussed in Sec. IV.

Note that the tube dimensions remained unchanged, while orifices with different diameters were used. Therefore, the two cases studies are not strictly geometrically similar, since the area ratio between the orifice and tube cross section was different. One of the main consequences is that the recirculation regions in these two cases are different. This could contribute to the differences between the two cases observed in Fig. 17.

Figure 18 shows the source spectral function versus St number for constant values of the Reynolds number for both orifice diameters. As mentioned already, the influence of Re number is small, and the source function levels for the larger orifice diameter are greater than for the smaller orifice diameter. A regression, shown in the figure, suggests a St^{-3} dependence of the source spectral function on the St number for $\mathrm{St}<0.9$, and a St^{-5} dependence for $\mathrm{St}>2.5$. Considering the $(\rho U^2)^2 d/U$ factor, these correspond to U^6 and U^8 dependences on velocity for the sound pressure spectra, respectively. The source function transitioned from the St^{-3} dependence to a St^{-5} dependence over Strouhal number values between 1 and 2.5.

The frequency dependence of the sound pressure spectra can be deduced from the basic trends of the source and radiation functions. At low frequencies, the M function exhibits a f^2 dependence. If the jet velocity is very small, the F function exhibits a f^{-5} dependence, the Strouhal number being large. The sound pressure spectra therefore follows a f^{-3} dependence, as shown in Fig. 3. As the jet velocity increases, the Strouhal number decreases. When the Strouhal number is small enough the F function then follows a f^{-3} law, and the sound pressure spectra a f^{-1} law. At higher frequencies, the radiation efficiency becomes approximately He^4. Accordingly, the sound pressure spectra exhibit a f^{-1} dependence.

The source function was compared with the nondimensional spectra obtained by Nelson *et al.* (1981). In their study, different formulations were used for the planar wave frequency range and the multimode frequency range. Over the planar wave range, the sound power spectra were scaled by $(1/\rho c)\rho^2U^4$, while over the multimode range the spectra were scaled by $(1/\rho c)\rho^2U^4\mathrm{He}^2$. These are similar to the $\rho^2U^4\mathrm{He}^2$ and $\rho^2U^4\mathrm{He}^4$ scaling laws for sound pressure spectral density in this study, except they considered a dipole source instead of a quadrupole source. They therefore obtained a nondimensional $\frac{1}{3}$-oct spectrum which showed a 20 dB decay per decade of St number, or a St^{-2} dependence, for St numbers above 0.2. This corresponds to a St^{-3} dependence of the spectral density. This result is in contrast with the St^{-5} dependence of the F function for a quadrupole source (for St numbers above 2.5) observed in the present study.

It should be noted that the source spectral distribution function, as discussed before, describes the frequency distribution of the propagating component of the turbulence energy. The energy in the turbulence associated with zero dilatation velocity can only produce near-field pressure fluctuations, and cannot propagate as sound in the far field.

C. Sound radiation in a finite length tube

The experiment was repeated with the downstream anechoic termination removed. The orifice had a 0.381-cm diameter. The jets discharged directly into open space from the end of the downstream rectangular tube (22.5 cm in length). This significantly changed the acoustic loading of the system, as well as the system acoustic response function.

Sound pressure spectra were measured downstream of the orifice, for different jet velocities and speed of sound. Figure 19 shows one typical sound spectrum, for $\Delta p=12$ cm

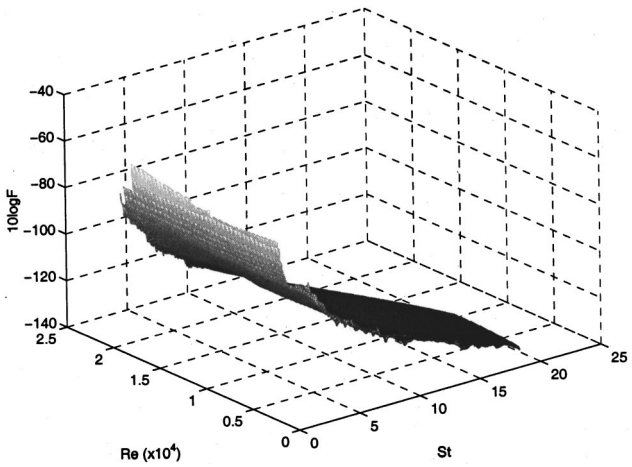

FIG. 20. Source spectral distribution for the case of a finite length tube downstream of the orifice plate.

H_2O and air as the medium. The high frequency part of the spectrum was similar to that obtained for the case with anechoic termination. However, the low frequency part was quite different. The peaks and resonance in the spectrum suggest a different system acoustic response function.

The spectral decomposition method was then used to separate the three different functions. The source distribution function F, shown in Fig. 20, is similar to that for the case with anechoic termination. The fluctuations at low Reynolds number are believed to be due to numerical errors. Figure 21 shows the function $10\log G_1$. Also shown in the figure are two curves He^2 for low He numbers ($\mathrm{He}<0.45$) and He^4 for high He numbers ($\mathrm{He}>0.45$). The good match of these two curves with the shape of the G_1 function suggests a radiation efficiency of He^2 and He^4 at low He numbers and high He numbers, respectively.

The G_1 function frequency distribution was similar to that of the measured sound pressure spectrum. For comparison, the system acoustic response function, G_{exp}, was calculated using the same method as that for the case with anechoic termination. The G function, obtained by removing the He^2 trend from the G_1 function, was compared to the G_{exp} function, which is shown in Fig. 22. A very good agreement was obtained for the He number lower than the critical value corresponding to the cut-on frequency of the acoustic higher modes. The discrepancies at high He numbers are expected since the plane wave assumption is no longer valid. This good agreement at low He numbers also indicates a radiation efficiency function M in the form of He^2.

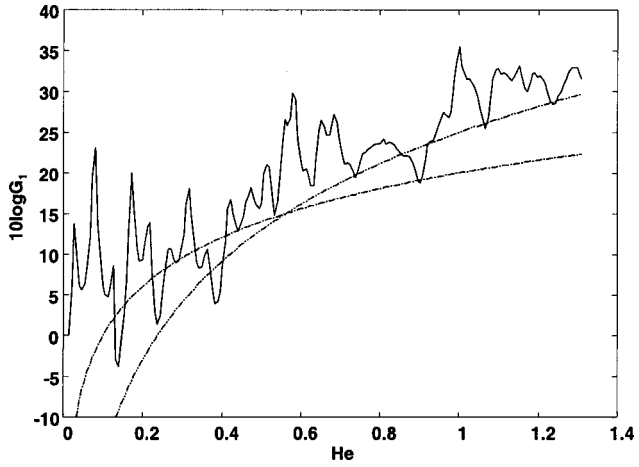

FIG. 21. G_1 function obtained for the case of a finite-length tube. ———: $10\log G_1$, $d=0.381$ cm; —·—·—·—: 20logHe; –··–: 40logHe.

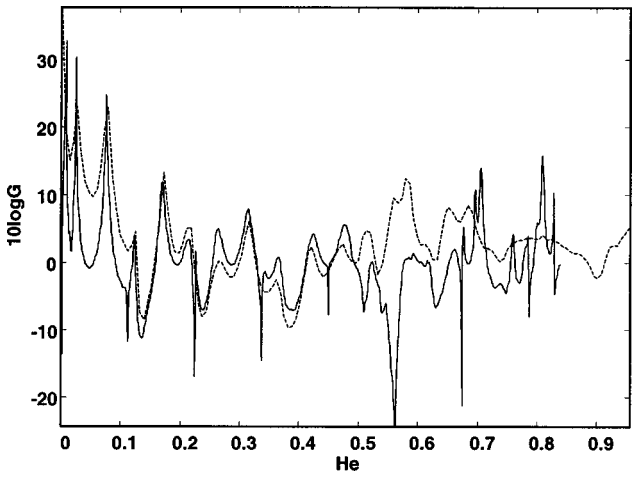

FIG. 22. Comparison between the G function obtained by removing the He^2 trend from the G_1 function, and the G_{exp} function obtained experimentally. The orifice plate was connected to a finite length tube downstream. ———: system acoustic transfer function; — — —: $10\log G$.

The M function was also obtained by subtracting the G_{exp} function from the G_1 function, as shown in Fig. 16. The He^2 curve matches the M function well at low He numbers. Since the G_{exp} function is not accurate at high He number, the agreement between the He^4 curve and the M function is poor, as expected.

The variation of the F function with the Re number for constant St numbers and St number for constant Re number are respectively shown in Figs. 17 and 18 in comparison with the F function obtained for the same orifice diameter with anechoic termination. These two F functions matched very well except at very low St number, over which the F function for finite length tube had a lower value than that for the case with anechoic termination. This difference may be due to the numerical error, i.e., there is not enough overlapping at very low St numbers. The two F functions showed a similar dependence on the St number and Re number. The effects of possible interaction between the flow field and acoustic loading were thus negligible.

D. Sound power

Sound power can be determined by integrating Eq. (10) over the entire frequency range and dividing by the characteristic impedance, ρc. At low frequencies where only plane waves propagate, $M\sim\mathrm{He}^2$. With $\mathrm{He}=Ma\cdot\mathrm{St}$, this He^2 term can be converted into a Ma^2 term. Ignoring the Re dependence, the integration then leads to a sound power of the order $\rho U^3 Ma^3$. For the high frequency component, $M\sim\mathrm{He}^4$. Following a similar approach, the sound power is of the order $\rho U^3 Ma^5$. These observations are consistent with the derivation by Davies *et al.* (1968).

VII. CONCLUSIONS

Experiments were performed to study the characteristics of sound generated by confined stationary jets through circular orifices. Nondimensional sound spectra were formulated as the product of a source spectral distribution function, a radiation efficiency function, and a system response function which describes the acoustic effects present in the tube. The source function is a function of both St and Re numbers, and the other two are functions of He number only. A spectral decomposition method based on a source-filter model was used to separate these three functions. Experiments were conducted for two downstream tube configurations and two orifice-tube dimension ratios. The results show that the system response function agrees well with the acoustic transfer function between the sound pressure spectra in the source and observer locations in the tube. The tube configuration has little effect on the source function and radiation efficiency function, which confirms the negligible interaction between the flow and acoustic loadings and the source-filter model. For a straight downstream tube configuration in this study, the radiation efficiency is similar to that of sound generation by a quadrupole source in tubes. This indicates that the dipole source contribution, which is due to the fluctuating axial force applied by the orifice wall, is negligible, and that the flow coming out of the straight orifice is very stable. This radiation efficiency also leads to a $\rho U^3 Ma^3$ and $\rho U^3 Ma^5$ scaling for the sound power at low and high frequencies, respectively. The source function obtained for confined jets having two different orifice diameters matched very well, within 2–3 dB difference. Analysis of the source spectral distribution function showed that Reynolds number effects were nearly negligible over the range 2000 to 20 000, except for a very slow increase of the source strength with the Reynolds number. The source distribution function was found to decrease with the Strouhal number as approximately St^{-3}, at very low Strouhal number and St^{-5} at high Strouhal number.

ACKNOWLEDGMENTS

This study was supported by Grant No. 5 RO1 DC03577-02 from the National Institute of Deafness and Other Communication Disorders, National Institutes of Health.

Bartenwerfer, M., and Agnon, R. (**1976**). ''On the influence of viscosity of the working fluid on the sound production of centrifugal fans,'' DFVLR Report, DLR-FB, 76-30.

Bartenwerfer, M., Agnon, R., and Gikadi, T. (**1976**). ''An experimental investigation on noise production and noise propagation in centrifugal fans,'' DFVLR Report, DLR-FB, 76-14.

Blake, W. K. (**1986**). *Mechanics of Flow-induced Sound and Vibration* (Academic, New York).

Davies, H. G., and Ffowcs Williams, J. E. (**1968**). ''Aerodynamic sound generation in pipe,'' J. Fluid Mech. **32**(4), 765–778.

Flanagan, J. L. (**1965**). *Speech Analysis, Synthesis and Perception* (Academic, New York).

Harper, V. H. (**2000**). ''Respiratory tract acoustical modeling and measurements,'' Ph.D. thesis, Purdue University, West Lafayette, IN.

Howe, M. S. (**1998**). *Acoustics of Fluid-structure Interactions* (Cambridge U.P., Cambridge).

Hubbard, H. H. (**1994**). *Aeroacoustics of Flight Vehicles: Theory and Practice. Vol. 1: Noise Sources* (Acoustical Society of America, New York).

Landau, L. D., and Lifshitz, E. M. (**1997**). *Fluid Mechanics* (Butterworth Heinemann, Boston).

Lighthill, M. J. (**1952**). ''On sound generated aerodynamically—I. General theory,'' Proc. R. Soc. London, Ser. A **211**, 564–587.

Meyer-Eppler, W. (**1953**). ''Zum Erzeugungsmechanismus der Geräuschlaute,'' Z. Phonet. all. Sprachwissensch. **7**, 196–212.

Mongeau, L., Thompson, D. E., and McLaughlin, D. K. (**1995**). ''A method for characterizing aerodynamic sound sources in turbomachines,'' J. Sound Vib. **181**(3), 369–389.

Neise, W. (**1975**). ''Application of similarity laws to the blade passage sound of centrifugal fans,'' J. Sound Vib. **43**(1), 61–75.

Nelson, P. A., and Morfey, C. L. (**1981**). ''Aerodynamic sound production in low speed flow ducts,'' J. Sound Vib. **79**(2), 263–289.

Pierce, A. D. (**1989**). *Acoustics: An Introduction to its Physical Principles and Applications* (Acoustical Society of America, New York).

Seybert, A. F., and Ross, D. F. (**1977**). ''Experimental determination of acoustic properties using a two-microphone random-excitation technique,'' J. Acoust. Soc. Am. **61**, 1362–1370.

Shadle, C. H. (**1986**). ''The acoustics of Fricative Consonants,'' MIT, Cambridge, MA, RLE Technical Report 506, March 1986.

Stevens, K. N. (**1998**). *Acoustic Phonetics* (The MIT Press, Cambridge, Massachusetts).

Weidemann, J. (**1971**). ''Analysis of the relations between acoustic and aerodynamic parameters for a series of dimensionally similar centrifugal fan rotors,'' NASA Technical Translation TT F-13, 798.

Zhang, Z., Mongeau, L., and Frankel, S. H. (**2002**). ''Experimental verification of the quasi-steady assumption for aerodynamic sound generation by pulsating jets in tubes,'' J. Acoust. Soc. Am., in press.

Zhao, Z., Frankel, S. H., and Mongeau, L. (**2001**). ''Numerical Simulations of Sound from Confined Pulsating axisymmetric Jets,'' AIAA J. **39**(10), 1868–1874.